A novel joint sparse partial correlation method for estimating group functional networks

Article *in* Human Brain Mapping · December 2015

DOI: 10.1002/hbm.23092

3 authors, including:

Xiaoyun Liang
University of Melbourne
50 PUBLICATIONS **169** CITATIONS
SEE PROFILE

Alan Connelly
The Florey Institute of Neuroscience and Men…
296 PUBLICATIONS **14,601** CITATIONS
SEE PROFILE

A Novel Joint Sparse Partial Correlation Method for Estimating Group Functional Networks

Xiaoyun Liang,[1]* Alan Connelly,[1,2,3] and Fernando Calamante[1,2,3]

[1]*Florey Institute of Neuroscience and Mental Health, Heidelberg, Victoria, Australia*
[2]*Florey Department of Neuroscience and Mental Health, University of Melbourne, Melbourne, Victoria, Australia*
[3]*Department of Medicine, Austin Health and Northern Health, University of Melbourne, Melbourne, Victoria, Australia*

Abstract: Advances in graph theory have provided a powerful tool to characterize brain networks. In particular, functional networks at group-level have great appeal to gain further insight into complex brain function, and to assess changes across disease conditions. These group networks, however, often have two main limitations. First, they are popularly estimated by directly averaging individual networks that are compromised by confounding variations. Secondly, functional networks have been estimated mainly through Pearson cross-correlation, without taking into account the influence of other regions. In this study, we propose a sparse group partial correlation method for robust estimation of functional networks based on a joint graphical models approach. To circumvent the issue of choosing the optimal regularization parameters, a stability selection method is employed to extract networks. The proposed method is, therefore, denoted as JGMSS. By applying JGMSS across simulated datasets, the resulting networks show consistently higher accuracy and sensitivity than those estimated using an alternative approach (the elastic-net regularization with stability selection, ENSS). The robustness of the JGMSS is evidenced by the independence of the estimated networks to choices of the initial set of regularization parameters. The performance of JGMSS in estimating group networks is further demonstrated with in vivo fMRI data (ASL and BOLD), which show that JGMSS can more robustly estimate brain hub regions at group-level and can better control intersubject variability than it is achieved using ENSS. *Hum Brain Mapp 00:000–000, 2015.* © 2015 Wiley Periodicals, Inc.

Key words: functional connectivity; sparse partial correlation; connectome; graphical models; arterial spin labeling

INTRODUCTION

Advances in MRI have provided arguably unique tools to probe brain structure and function non-invasively. The brain connectome, a comprehensive map of neural connections in the brain, has recently emerged as an area of major interest in neuroimaging and neuroscience. Increasing evidence suggests that the human brain can be

Additional Supporting Information may be found in the online version of this article.

Contract grant sponsor: National Health and Medical Research Council (NHMRC) of Australia, Australian Research Council (ARC), and Victorian Government's Operational Infrastructure Support Program.

*Correspondence to: Xiaoyun Liang, Florey Institute of Neuroscience and Mental Health, Melbourne Brain Centre, 245 Burgundy St., Heidelberg, Victoria, 3084, Australia.
E-mail: x.liang@brain.org.aui, imagetechliang@gmail.com

Received for publication 3 September 2015; Revised 3 December 2015; Accepted 6 December 2015.

DOI: 10.1002/hbm.23092
Published online 00 Month 2015 in Wiley Online Library (wileyonlinelibrary.com).

modeled as a complex network [Stam and Reijneveld, 2007]. Advances in graph theory have provided powerful quantitative tools to characterize brain networks and connectivity [Latora and Marchiori, 2001; Sporns and Zwi, 2004; Stam and Reijneveld, 2007]. Network metrics allow for the quantitative comparison of connectivity pattern among groups, such as between healthy subjects and patients. They have transformed our understanding of brain networks in the healthy brain, and the effects of their disruption due to a disease process.

Among the existing techniques for mapping functional networks, resting-state Blood Oxygenation Level Dependent (BOLD) fMRI is the most commonly used, due to its simple MRI acquisition sequence and relative high spatial resolution. As an alternative, arterial spin labeling (ASL) fMRI has been also successfully applied to map resting-state functional networks [Liang et al., 2012a, 2013, 2014]. ASL has been shown to offer a number of potential advantages compared with BOLD fMRI (e.g. quantitative measurement of cerebral blood flow, and reduced intersubject variability [Aguirre et al., 2002, Wang et al., 2003], but it is often also associated with a reduced temporal and spatial resolution and signal-to-noise ratio (SNR) [Calamante et al., 1999]. Therefore, both BOLD and ASL can have important complementary roles in the study of the functional connectome.

Pearson Correlation Versus Partial Correlation

A key step in the analysis of functional networks is the calculation of the degree of connectivity. This has been estimated mainly through calculating Pearson correlation coefficients, c_{ij}, between the mean time series of regions i and j. The resulting correlation coefficients are then often thresholded to create connectivity matrices, which can be either binarized or weighted. In this way, interactions between multiple brain regions can be characterized. However, this approach measures the general relationship between two regions without taking account of the influence of the others. To address this issue, partial correlations can be employed [Hampson et al., 2002, Salvador et al., 2005], which measure the degree of association between two brain regions while removing the effect of all the other regions. This, therefore, allows direct and indirect connectivity to be distinguished [Eichler et al., 2003].

Partial correlations can be obtained by estimating inverse covariance (ICOV) matrices [Dempster, 1972]. Essentially, non-zero entries of the ICOV matrix indicate non-zero partial correlations. However, these are always ill-posed problems. This issue has been addressed mainly by imposing sparse constraints as regularization, given that it is generally accepted that brain networks are sparse [Achard and Bullmore, 2007, Bullmore and Sporns, 2012; Liang et al., 2015]. Specifically, this has been solved by using norm regularization, such as L1-norm [Tibshirani, 1996] and a combination of L1- and L2-norm, called elastic net (EN) regularization [Zou and Hastie, 2005]. While both sparse constraints have been shown to be capable of extracting interpretable sparse networks, EN regularization has been demonstrated to estimate functional connectivity more robustly than L1-norm [Ryali et al., 2012]. This is mainly due to the intrinsic limitations of L1-norm in comparison with EN regularization: when there are several highly correlated variables that are all relevant to the output variable, the L1-norm tends to pick one or a few of them by shrinking the rest to 0 [Zou and Hastie, 2005]. In contrast, L2-norm is able to select groups of correlated variables, but all variables selected will be different from 0. Therefore, L2-norm produces non-sparse coefficients, so L2-norm itself might not be feasible to estimate sparse networks [Tibshirani, 1996]. Note, however, that this does not imply that L2-norm is incapable of estimating brain networks. In fact, it was shown that L2-norm can achieve high accuracy and reproducibility across subjects in estimating brain networks without relying on sparsity [Rasmussen et al., 2012]. In an alternative way, to estimate sparse networks, Rasmussen and colleagues proposed an approach that employed logistic regression combined with EN regularization, showing the capability of that method in estimating sparse brain networks [Rasmussen et al., 2012].

Group-Level Versus Individual Level Analyses

Generally, functional networks can be analyzed at either individual- or group-level. While the former is important for many applications, including subject-specific treatment (e.g. so-called precision medicine) and to study intersubject variability, group-level network analysis is also a very powerful approach. For example, to probe the mechanism of complex brain function and how networks change across disease conditions and mental states, brain functional networks at group-level are of great interest for researchers [Simpson et al., 2012]; in many of these applications, it is the group average network that is of interest. Furthermore, the relatively low SNR of fMRI data often limits the robustness of individual network results, while still allowing for reliable estimates of the average network in a given group. Group-level networks are also of interest for group comparison studies, for which significant differences between groups can be statistically tested.

For group-level studies, it is generally assumed that all subjects are from a relatively homogeneous group that shares a common structure, while containing intersubject variability related to biological variations, which has biological importance in modeling diseases and needs to be retained. However, confounding contributions of intersubject variability, such as physiological noise (i.e. heartbeat, respiration, vascular noises, etc.), and other sources of noise (sampling noise, processing noise, motion artifacts, etc.), could unfavorably conceal significant group differences, which are deemed detrimental for group comparison

studies. Therefore, an approach that could favorably control for confounding variation while minimally compromising biological variation is therefore appealing.

In group-level analyses, networks are usually averaged across subjects [Achard et al., 2006, Liang et al., 2014]. While more sophisticated approaches can be applied, such as *t*-tests applied to Fisher's *z*-transform [Buckner et al., 2011], this is inevitably affected by intersubject variability as related to confounding variations, which is further exacerbated by relatively low SNR (e.g. for ASL data). Furthermore, it is not trivial to determine the optimal threshold across subjects, given that there is no consensus on how to choose the optimal threshold that binarizes connectivity matrices into adjacency matrices at individual-level. So far, there have been a few existing methods that aim either to jointly estimate multiple functional networks from multiple categories [Chiquet et al., 2011; Guo et al., 2011], or to estimate individual functional networks by enforcing constraints (i.e. population prior or anatomical information) to account for intersubject variability [Ng et al., 2013; Varoquaux et al., 2010a,b]. However, these studies do not generally focus on the estimation of group-level functional networks from within homogeneous groups.

In this study, we propose a novel sparse group partial correlation method for simultaneously estimating individual networks from a homogeneous group of subjects; we aim to control for confounding variations that mainly possess non-sparsity, and to minimally compromise biological variations (i.e. sparsity), by employing a biologically-plausible joint sparse constraint (Note that this approach might not effectively control "sparse-like" confounding variations—see Discussion section for further information). As such, the levels at which the confounding variations characterized by nonsparsity are controlled and biological variations are retained are largely data-driven. The proposed method is developed based on a recently proposed joint graphic models (JGM) approach [Danaher et al., 2013], which borrows strength across classes and estimates common structures across classes, as well as specific edges exclusively belonging to each class; i.e. it enforces the same sparse pattern across classes but allows for variability in edge values. While the proposed method is adapted from JGM, it has a very different role in estimating functional networks, i.e. it aims to estimate individual networks sharing common network structures across a homogeneous group while still allowing intersubject biological variability. In this regard, the statistical power of group comparison studies should be enhanced by controlling the total confounding variance that inherently exists with extant methods.

Specifically, implementation of the proposed method involves model selection, i.e. choosing optimal regularization parameters. While the Akaike information criterion (AIC) [Akaike, 1974] or the Bayesian information criterion (BIC) [Schwartz, 1978] potentially could be used, these can lead to poor model estimation for data with small sample size and high dimension [Hansen et al., 1999; Zhang and Shen, 2010]. We propose to address the issue by employing the method of stability selection [Meinshausen and Buhlmann, 2010; Rasmussen et al., 2012; Ryali et al., 2012] that subsamples data across a range of regularization parameters rather than seeking a single set of optimal parameters. In this context, the proposed method is denoted as JGMSS (Joint Graphical Model with Stability Selection). To assess performance, the proposed method is applied to simulated data, and also applied to two in vivo fMRI datasets (ASL and BOLD fMRI datasets). For comparison, the same data (both simulated and in vivo) were also analyzed using the EN method combined with stability selection (ENSS).

MATERIALS AND METHODS

The JGMSS Method

The graphical model

For fMRI data M with matrix size $n \times p$, where n is the number of time points and p is the number of brain regions, we assume that $m_1, \ldots, m_n \in R^p$ (m_i is the ith row of matrix M) follow a normal distribution with mean $\mu \in R^p$ and covariance $\Sigma \in R^{p \times p}$. Estimating functional connectivity amounts to estimating the *ICOV* matrix Σ^{-1} via maximum likelihood of the following expression [Danaher et al., 2014]:

$$\frac{n}{2}(\log\det\Sigma^{-1} - \mathrm{Tr}(S\Sigma^{-1})), \tag{1}$$

where Tr represents the trace of a matrix, det its determinant, and S the empirical covariance matrix. The maximum likelihood estimate of S^{-1} can be obtained by maximizing Eq. (1) with respect to Σ^{-1}.

To obtain sparse estimation of functional connectivity, Eq. (1) can be reformatted by taking a penalized log-likelihood approach:

$$\max_X \{\log\det X - \mathrm{Tr}(SX) - \lambda\|X\|_1\}, \tag{2}$$

Where λ is a nonnegative parameter, X is an estimate of Σ^{-1}, and $||\cdot||_1$ the L1-norm, with 0 at ith and jth entry of X indicating that the regions i and j are conditionally independent given the other regions.

The proposed JGMSS approach

In a nutshell, the proposed method is applied across a group of subjects. It is assumed that K datasets, $D^{(1)}, \ldots, D^{(K)}$, are obtained, where $D^{(k)}$ is a $n_k \times p$ matrix, with n_k representing time points of the fMRI dataset k, and p is the number of brain regions. The empirical covariance matrix for $D^{(k)}$ is calculated as follows:

$$S^{(k)}=\frac{1}{n_k}(D^{(k)})^T D^{(k)}. \quad (3)$$

Similar to Eq. (2), the ICOV matrices can be estimated by solving the following equation:

$$\max_X \sum_{k=1}^{K} n_k(\log\det X^{(k)}-\mathrm{Tr}(S^{(k)}X^{(k)}))-P(\{X\}), \quad (4)$$

with the constraint that all $X^{(k)}$ are positive definite, where $P(\{X\})$ is the group graphical-lasso constraint [Danaher et al., 2013]:

$$P(\{X\})=\lambda_1\sum_{k=1}^{K}\sum_{i\neq j}\left|x_{ij}{}^{(k)}\right|+\lambda_2\sum_{i\neq j}\sqrt{\sum_{k=1}^{K}x_{ij}{}^{(k)2}}, \quad (5)$$

where λ_1 and λ_2 are nonnegative regularization parameters. This approach has the benefit that, by applying the penalty, it tends to estimate a similar pattern of sparsity across the ICOV matrices of all the K datasets.

The alternating direction method of multipliers (ADMM) approach. Equation (4) can be reformatted as follows, and then solved by using ADMM [Boyd et al., 2010]:

$$\min_{\{X\},\{Z\}} \sum_{k=1}^{K} n_k(\mathrm{Tr}(S^{(k)}X^{(k)})-\log\det X^{(k)})+P(\{Z\}), \quad (6)$$

subject to the constraints that $X^{(k)}$ is positive definite and $Z^{(k)}=X^{(k)}$ for $k=1,\ldots K$. The ADMM algorithm for estimating the group-level sparse ICOV matrices can be formulated by introducing a dual variable, $U=\{U^{(1)},\ldots,U^{(K)}\}$, as follows [Boyd et al., 2010; Danaher et al., 2013]:

Repeat the following steps until convergence ($i=1,2,3,\ldots$):

$$1.\ X_{(i+1)}^{(k)}=\arg\min_X\Big(\sum_{k=1}^{K}n_k(Tr(S^{(k)}X^{(k)})-\log\det X^{(k)})+\frac{1}{2}\sum_{k=1}^{K}\|X^{(k)}-Z_{(i)}^{(k)}+U_{(i)}^{(k)}\|_F^2\Big) \quad (7a)$$

$$2.\ Z_{(i+1)}^{(k)}=\arg\min_Z\left(P(\{Z\})+\frac{1}{2}\sum_{k=1}^{K}\|X_{(i+1)}^{(k)}-Z^{(k)}+U_{(i)}^{(k)}\|_F^2\right) \quad (7b)$$

$$3.\ U_{(i+1)}^{(k)}=U_{(i)}^{(k)}+X_{(i+1)}^{(k)}-Z_{(i+1)}^{(k)} \quad (7c)$$

where $\|\bullet\|_F$ is the Frobenius norm, i.e. the square-root of the sum of the squares of the entries.

According to the first-order-optimality condition, the solution to Eq. (7a) can be obtained by setting the first-order derivatives to zero. For $k=1,\ldots,K$, setting the first derivative of Eq. (7a) to zero leads to the following expression:

$$(Z_{(i)}^{(k)}-U_{(i)}^{(k)})/n_k-S^{(k)}=X^{(k)}/n_k-(X^{(k)})^{-1}. \quad (8)$$

By using eigenvalue decomposition, the left-hand side of Eq. (8) can be rewritten as:

$$(Z_{(i)}^{(k)}-U_{(i)}^{(k)})/n_k-S^{(k)}=V^{(k)}\Lambda^{(k)}V^{(k)T} \quad (9)$$

where $\Lambda^{(k)}=\mathrm{diag}(\sigma_1{}^{(k)},\ldots,\sigma_{n_k}{}^{(k)})$, and $V^{(k)}V^{(k)T}=V^{(k)T}V^{(k)}=I$.

It is shown that $X^{(k)}$ in Eq. (8) has the same eigenvectors $V^{(k)}$ as in Eq. (9) [Witten and Tibshirani, 2009]. Letting $\Lambda^{(k)'}=\mathrm{diag}(\sigma_1{}^{(k)'},\ldots,\sigma_{n_k}{}^{(k)'})$ denote the matrix of eigenvalues of $X^{(k)}$, the following equation can be obtained from Eqs. (8) and (9):

$$\sigma_j{}^{(k)'}/n_k-1/\sigma_j{}^{(k)'}=\sigma_j{}^{(k)} \quad (10)$$

The jth eigenvalue $\sigma_j{}^{(k)'}$ of $X^{(k)}$ can then be calculated:

$$\sigma_j{}^{(k)'}=(\sigma_j{}^{(k)}\times n_k+\sqrt{(\sigma_j{}^{(k)})^2\times n_k{}^2+4n_k})/2, \quad (11)$$

then updating $X^{(k)}$ as follows,

$$X^{(k)}=V^{(k)}\Lambda^{(k)'}V^{(k)T}. \quad (12)$$

The variable Z can be sequentially updated [Boyd et al., 2010]:

$$Z_{(i+1),j}^{(k)}=T(X_{(i+1),j}^{(k)}+U_{(i),j}^{(k)},\lambda_1)\left(1-\lambda_2/\sqrt{\sum_{k=1}^{K}T(X_{(i+1),j}^{(k)}+U_{(i),j}^{(k)},\lambda_1)^2}\right)_+, \quad (13)$$

where T is the soft-thresholding function, $T(U,\lambda)=\mathrm{sgn}(U)\max(0,|U|-\lambda)$, and $x_+=\max(x,0)$. For $k=1,\ldots,K$, $U_{(i+1)}^{(k)}$ can be updated then according to Eq. (7c).

Estimation of networks using stability selection. There are two regularization parameters,λ_1 and λ_2, that need to be determined. Rather than choosing an optimal model by using AIC or BIC, the current study employs a recently proposed statistical method, namely stability selection [Meinshausen and Buhlmann, 2010]. With this approach, data are perturbed many times and any connections that occur in a large fraction of the resulting selection sets are chosen. Specifically, for a given pair of parameters $(\lambda_1,\lambda_2)\in\Lambda\subseteq R^+$, with Λ the set of regularization parameters chosen, estimating brain connections (i,j), i.e. (binarized) edges between regions i and j, at group-level amounts to estimating the set

$$S^{\lambda_1,\lambda_2}=\begin{cases}1 & \text{if } Z_g(i,j)\neq 0 \text{ and } i\neq j\\ 0 & \text{otherwise}\end{cases} \quad (14)$$

with Z_g [see Eq. (13)], the estimated ICOV matrix at group-level, defined as follows:

$$Z_{g(i,j)} = \begin{cases} 1, & Z_{(i,j)}^{(k)} = 1 \text{ for } k = 1, \ldots, K \\ 0, & \text{otherwise} \end{cases} \quad (15)$$

Given that a common network is sought, for the current implementation of the method, a stringent rule was applied where only connections present across all subjects were considered as true connections. For a given pair of parameters (λ_1, λ_2), the probability $\hat{P}_{i,j}^{\lambda_1,\lambda_2}$ for one connection between brain regions i and j to be selected can be obtained by randomly sampling a subset of contiguous points (in our case, four points) from the n number of time points. By setting a threshold, $0.5 < P_{thr} < 1$, the set of stable connections, i.e. all estimated connections, can be obtained as follows [Meinshausen and Buhlmann, 2010]:

$$\hat{S}^{stable} = \begin{cases} 1 & \text{if } \max_{(\lambda_1,\lambda_2)\in\Lambda} \hat{P}_{i,j}^{\lambda_1,\lambda_2} \geq P_{thr} \\ 0 & \text{otherwise} \end{cases}. \quad (16)$$

Furthermore, the bound on the expected number of false connections (N_{FC}) can be specified as follows [Meinshausen and Buhlmann, 2010]:

$$E(N_{FC}) = \frac{1}{(2P_{thr} - 1)} \frac{{q_\Lambda}^2}{C} \quad (17)$$

where q_Λ is the average number of selected connections across the set Λ, and C is the number of all possible connections, i.e. $C = p(p-1)/2$, with p the number of brain regions. The per-comparison error rate (PCER = $E(N_{FC})/C$) is employed to control falsely selected connections.

Matlab code to perform the proposed method can be downloaded from http://www.brain.org.au/software/index.html.

Simulation

To assess the robustness of the proposed method, we first simulated three small-world networks with varying percentages of connections $(r = 16, 24, 32)$ with a connection probability of 0.01 [Watts and Strogatz, 1998]. Three covariance matrices were then generated with zeros corresponding to no connections and values from a normal distribution on [0.6,1] corresponding to connections. Data were simulated with 50 regions at 56 time points by following reference [Peng et al., 2009]. (Note: the number of time points was chosen to be the same as for the in vivo ASL data in our study—see protocol below). For each r value, the procedure was repeated 10 times to generate 10 datasets, i.e. equivalent to 10 subjects.

In Vivo Data: Imaging Protocol

Subjects

Ten healthy subjects were recruited to participate in the ASL study, and eight for the BOLD study. Data were acquired on a 3 T Siemens Tim Trio scanner (Erlangen, Germany) with a 12-channel head coil. All subjects provided written, informed consent, and all protocols were approved by the local Institutional Review Board.

Data acquisition

ASL data. Resting-state ASL data were acquired using a previously published 3D GRASE pCASL sequence [Liang et al., 2012a], TR/TE = 3,750/56ms, resolution = 4 × 4 × 6 mm^3, 20 axial slices, matrix size = 64 × 51. Labeling position was determined according to [Aslan et al., 2010], with labeling duration = 1,284 ms. Background suppression (BS) was achieved using inversion-times of 1,913 ms and 523 ms [Garcia et al., 2005]. For each subject, 112 images (56 label/control pairs) were acquired. Based on previous ASL findings for fMRI [Gonzalez-At et al., 2000] and a resting-state functional connectivity [Liang et al., 2012a], a short post-labeling delay (PLD) ASL sequence is preferred to a long PLD sequence due to the relatively higher SNR of the former. We therefore used a PLD = 600 ms.

Anatomical scans and ASL reference. Anatomical reference images were acquired using a Magnetization-Prepared-Rapid-Gradient-Echo (MPRAGE) sequence, with the following relevant parameters: TR/TE/TI = 1,900/2.55/900 ms, flip-angle = 9°, 1mm isotropic resolution, field-of-view = 256×256mm^2, 160 partitions. To aid with accurate registration, a reference scan (M_0) was acquired using the same parameters as those used for ASL, but without labeling or BS.

BOLD data. Resting-state BOLD fMRI data were acquired with a gradient-echo echo-planar imaging (EPI) sequence (TR/TE = 3,000/30 ms, voxel size: 3 mm isotropic, 44 slices, 100 volumes).

Image analysis

ASL data. Preprocessing. All image processing was carried out using SPM8 (Wellcome Department of Cognitive Neurology, http://www.fil.ion.ucl.ac.uk/spm). For each subject, preprocessing involved the following steps: (a) motion correction of ASL images, followed by spatially smoothing (6 mm isotropic Gaussian kernel), and subsequent co-registration (with the reference M_0 image) to the high-resolution anatomical image; (b) detrending; (c) perfusion images were obtained using Chebyshev high-pass filter followed by demodulation [Chuang et al., 2008]; (d) normalization to MNI standard space (resolution:3×3×3, matrix size: 61×73×61).

Independent component analysis (ICA). Following our previous work on resting state connectivity using ASL [Liang et al., 2014], ICA was used to remove intravascular 'artifacts', which are present in ASL data at short PLD [Gonzalez-At et al., 2000]; this minimizes the effect of intravascular effects on network metrics. This was conducted at an individual-level as implemented by FSL MELODIC software. See reference [Liang et al., 2014] for further details.

Region-wise time courses. The AAL template [Tzourio-Mazoyer et al., 2002] was used from brain parcellation. As done in our previous work [Liang et al., 2014], 84 regions out of 90 regions in the template were included (see [Liang et al., 2014] for detailed information). Region-wise mean time-courses were extracted across all 84 brain regions for each subject, yielding one dataset (matrix size: 56×84) for each subject.

BOLD data. ***Preprocessing.*** Image processing was performed using SPM8. For each subject, all BOLD images were preprocessed as follows: (a) motion-corrected, followed by detrending; (b) band-pass filtered (0.01−0.1Hz); (c) regressed out motion correction parameters, mean white matter and cerebrospinal fluid signal; then (d) coregistered to anatomical space; followed by (e) normalization to MNI standard space (resolution: 3×3×3, matrix size: 61×73×61).
Region-wise time courses. Ninety regions in the AAL template were included by excluding cerebellum [Tzourio-Mazoyer et al., 2002]. Region-wise mean time-courses were extracted across all voxels within each of the 90 brain regions for each subject, yielding one dataset (matrix size: 100×90) for each subject.

Implementation of JGMSS and ENSS

Simulation and ASL data

1. The JGMSS: A three-dimensional (3D) dataset with dimension size $n_k \times p \times K$ was constructed by combining all 10 normalized datasets ($K = 10$), with n_k=56, and p=50 (for simulated data) or 84 (for ASL data). To account for autocorrelation effects, time series were divided into consecutive and non-overlapping blocks [Ryali et al., 2012], with four time points in each block (for a total of $56/4 = 14$ blocks). Note that while no autocorrelation is expected in simulated data, the same procedures were applied to both simulated and in vivo data for consistency. A random subsampling was applied to obtain data with half the number of time points (4×14/2=28). The data were then analyzed using the JGMSS with a predefined range of regularization parameters $(\lambda_1, \lambda_2) \in \Lambda$, with lower bound $(\lambda_{1L}, \lambda_{2L})$ encompassing all possible connections and upper bound$(\lambda_{1U}, \lambda_{2U})$ yielding very few connections. The procedure was repeated 100 times for stability selection.
2. The ENSS: As with the JGMSS, data were divided into 14 blocks, with four time points in each block. Data were then randomly sampled to generate a new dataset with 28 time points. Functional networks were estimated using the ENSS at individual-level with a predefined range of regularization parameters $(\lambda_1, \lambda_2) \in \Lambda$ (see details for the JGMSS). The procedure was repeated 100 times for stability selection.

BOLD fMRI data

Both JGMSS and ENSS were also applied to BOLD fMRI data, with same procedures as implemented in simulations and ASL data, except for those related to the temporal dimension: due to the different size of the BOLD fMRI dataset (i.e. 100×90×8), time series were divided into 20 blocks, with $100/20 = 5$ time points in each block, and 50 time points for each randomly subsampled dataset.

Determination of P_{thr}

To investigate the legitimacy of choosing P_{thr} by setting *PCER*, an optimal estimate of network (with a maximum accuracy rate) was determined by changing P_{thr}; this was then employed to calculate optimal accuracy and sensitivity based on the ground truth for each simulation. For in vivo data, PCER = 0.05 was accordingly used to determine P_{thr} for controlling falsely selected connections.

Performance evaluation

To evaluate the proposed method in estimating the functional connectivity matrix at group-level, the following measures were applied to simulated data,

$$\text{Sensitivity} = \text{TP}/(\text{TP} + \text{FN})$$
$$\text{Accuracy} = (\text{TP}+\text{TN})/(\text{TP}+\text{FP}+\text{FN}+\text{TN})$$
$$\text{Specificity} = \text{TN}/(\text{TN}+\text{FP})$$

with TP the number of true positives, TN the number of true negatives, FP the number of false positives, FN the number of false negatives.

JGMSS sensitivity to regularization parameters

While the method of stability selection appeared to have low sensitivity to the initial set of regularization parameters in the study by Meinshausen and Buhlmann [2010], whether or not the JGMSS for fMRI data is dependent on the initial set of regularization parameters, Λ, remains to be determined. By varying the range of regularization parameters, i.e., the first 10 parameter pairs (λ_1, λ_2) out of 50 in total are sequentially removed from the set Λ, we estimated group–level functional networks from simulated data by using JGMSS, as well as the measures of sensitivity and accuracy. In this way, the extent to which the estimated functional networks depend on the initial set of regularization parameters was investigated.

Network degrees and hub regions

It has been shown that brain networks can be better characterized by an exponentially truncated power-law model than by other models [Achard et al., 2006, Hayasaka and Laurienti, 2010]; this model, therefore, was employed to fit the degree distribution of networks extracted from both ASL and BOLD in vivo data using JGMSS and ENSS. Subsequently, estimated fitting of R^2 values was employed as an evaluation tool to identify the more reliable networks in which more variance can be explained by the exponentially-truncated-power-law model.

Hub regions were identified as follows [Achard et al., 2006]. Firstly, the mean (and standard deviation) of degrees was calculated from each network estimated from ASL and BOLD data using JGMSS and ENSS, respectively. A degree threshold (mean + standard deviation) was subsequently employed to determine the hub regions for each network, i.e., any brain regions having degrees larger than the thresholds were chosen as hub regions.

Functional networks at group level using ENSS

For ENSS, due to non-normal distribution of the connectivity matrix (i.e. probability following stability selection with range of [0–1]), one-sample sign tests were employed instead of one-sample t-tests to determine true edges at a significant level of $P < 0.05$.

Quantification of intersubject variability

To evaluate the intersubject variability, functional networks were estimated at individual-level using JGMSS and ENSS. Since individual networks were estimated, $E(N_{FC})$ was individually estimated and one PCER was employed for each subject to control falsely selected connections. In addition to the selected P_{thr}, four additional thresholds were chosen to evaluate the intersubject variability across the range. To quantify the intersubject variability, the small-world index was calculated for the estimated global networks using the JGMSS and the ENSS by comparing the characteristic path length (L) and clustering coefficient (C) with the metrics measured in 1000 matched random networks (the same number of nodes, degrees and the same degree distribution as the real network) [Maslov and Sneppen, 2002; Sporns and Kotter, 2004; Sporns and Zwi, 2004]. The small-world index was calculated as follows:

$$\sigma = \gamma/\lambda \tag{14}$$

where $\gamma = C_{net}/C_{rand}$ and $\lambda = L_{net}/L_{rand}$, and the subscripts "net" and "rand" refer to the real network and to random networks respectively.

RESULTS

Group-Level Functional Network: Simulations

Figure 1a–c illustrate the performance of the proposed JGMSS method (left) in estimating group functional networks from simulated data in comparisons to the ENSS (middle) across the range of percentages of connections, $r = 16$, 24, and 32, with true networks (simulated ground truth) shown on the right. Note that the superiority of the proposed method for both $r = 16$ and 24 is demonstrated by both fewer false positives and fewer false negatives, while the superiority is less clear for $r = 32$.

Figure 2 shows the quantitative comparisons between the JGMSS and the ENSS across the simulated range, in terms of accuracy, sensitivity and specificity. JGMSS achieves consistently higher accuracy and sensitivity across the range than is achieved using ENSS. Meanwhile, JGMSS achieves comparable specificity to ENSS across the range (Fig. 2c). Overall, Figure 2 demonstrates that JGMSS can estimate group functional networks more accurately than ENSS.

The independence of the JGMSS on regularization parameters is manifested in terms of accuracy (Fig. 3a), sensitivity (Fig. 3b), and specificity (Fig. 3c). Moreover, the independence of the JGMSS to varying regularization parameters has been consistently demonstrated across the range of percentages of connections, r. This suggests that the estimation of functional networks for in vivo data is not affected by the choice of initial set of regularization parameters.

Group-Level Functional Network: In Vivo Data

Figure 4 shows the group functional network estimated from in vivo ASL (Fig. 4a) and BOLD (Fig. 4c) fMRI data with JGMSS by setting PCER = 0.05 to determine P_{thr}. For comparison, the estimated group functional networks from ASL and BOLD fMRI data using ENSS are shown in Figure 4b,d. The networks from either ASL or BOLD data are visually very similar between JGMSS and ENSS, with very similar network densities, i.e., ASL: 0.26 versus 0.29, BOLD: 0.18 versus 0.16, for JGMSS and ENSS, respectively.

Degree Distribution Fitting

Figure 5 shows degree distributions of functional networks extracted from ASL data using JGMSS (Fig. 5a) and ENSS (Fig. 5b), as well as from BOLD data using JGMSS (Fig. 5c) and ENSS (Fig. 5d). As expected, degree distribution (and therefore fitting outcomes) from ASL data is much noisier than from BOLD data, due to the lower SNR and fewer time points in ASL data. Degree distributions of networks using JGMSS are better fitted by the exponentially-truncated power-law degree distribution than using ENSS, with consistently higher R^2 values achieved by using JGMSS than ENSS.

Network Metrics at Individual Level

Figure 6 shows intersubject variability in terms of small world indices (associated means and standard deviations) calculated from within the following three groups of data: simulation (Fig. 6a), ASL (Fig. 6b) and BOLD (Fig. 6c) data across a range of P_{thr}. As expected, the results show that lower intersubject variability has been achieved by using JGMSS (red line) than by using ENSS (blue line) for these simulated data, and is also observed for in vivo data (ASL and BOLD data, see Supporting Information Fig. S1).

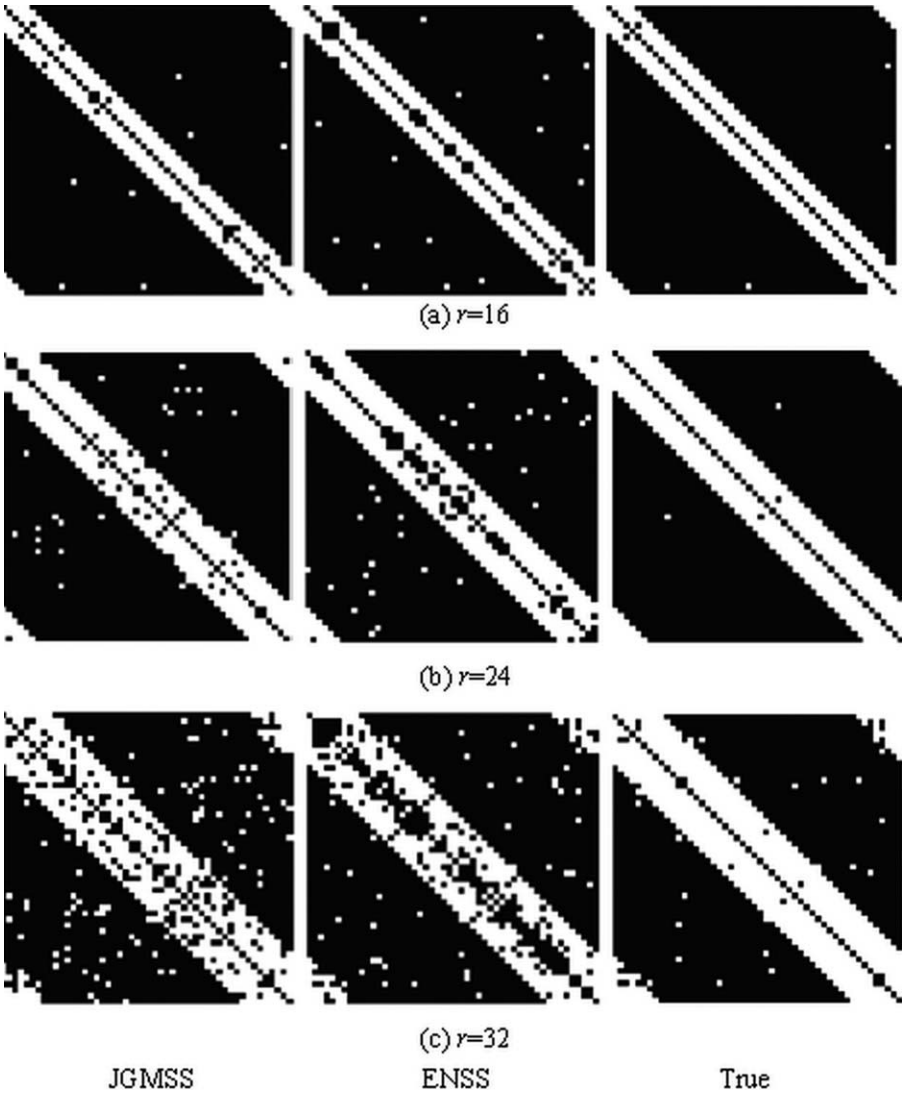

Figure 1.

Estimation of three simulated binary networks using the JGMSS (left column) and the ENSS (middle column) with true networks provided on the right: (**a**) $r = 16$; (**b**) $r = 24$; (**c**) $r = 32$, with r representing percentage of connectivity, black = 0, white = 1. Overall, these results illustrate the better performance of JGMSS in estimating group functional networks compared to ENSS. While the superiority of the proposed method is less clear for $r = 32$, the superiority for both $r = 16$ and 24 is demonstrated by both fewer false positives and fewer false negatives.

Visualization of Functional Networks

The estimated functional networks (84 and 90 nodes for ASL and BOLD data, respectively) are mapped onto the standard MNI template by using the BrainNet Viewer (www.nitrc.org/projects/bnv). Note: to better appreciate the detected degree differences, only hub regions are shown. Figure 7 visualizes brain hub regions calculated from networks estimated from ASL data using JGMSS (Fig. 7a) and ENSS (Fig. 7b), as well as from BOLD networks using JGMSS (Fig. 7c) and ENSS (Fig. 7d). Table I shows detailed hub region differences from ASL and BOLD between JGMSS and ENSS. Overall, JGMSS detected more hub regions than ENSS, i.e. 16 versus 12 from ASL data and 20 versus 15 from BOLD data, by using JGMSS and ENSS, respectively. All these listed potential hub regions except the Rolandic operculum (marked in red in Table I, which was erroneously detected using ENSS) have been previously reported as hub regions [Achard et al., 2006; Liao et al., 2013; Liang et al., 2014; Stam, 2014].

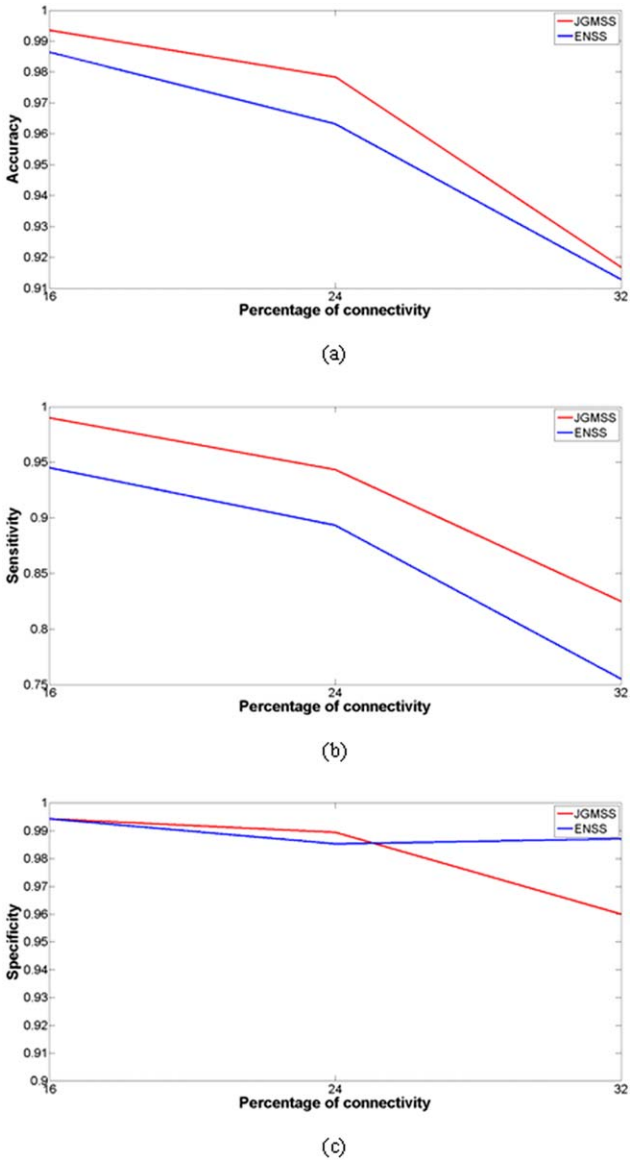

Figure 2.

Accuracy (**a**), sensitivity (**b**), and specificity calculated from the estimated networks using JGMSS and ENSS. For each method, the maximum achievable values of accuracy, as well as those corresponding values of sensitivity, for the three values of percentages of connection (r = 16, 24, 32) are plotted. These results clearly show that JGMSS achieves consistently higher accuracy and sensitivity in estimating group networks, while the achieved specificity is comparable for JGMSS and ENSS. [Color figure can be viewed in the online issue, which is available at wileyonlinelibrary.com.]

DISCUSSION

In this study, a novel sparse partial correlation method for estimating group functional connectivity from fMRI data has been proposed. The proposed JGMSS method adapts a joint graphical models approach [Danaher et al., 2013] to simultaneously estimate networks at individual-level and at group-level from within a homogeneous group through estimating partial correlations. Specifically, we aim to favorably enhance statistical power for facilitating the detection of significant group difference by largely

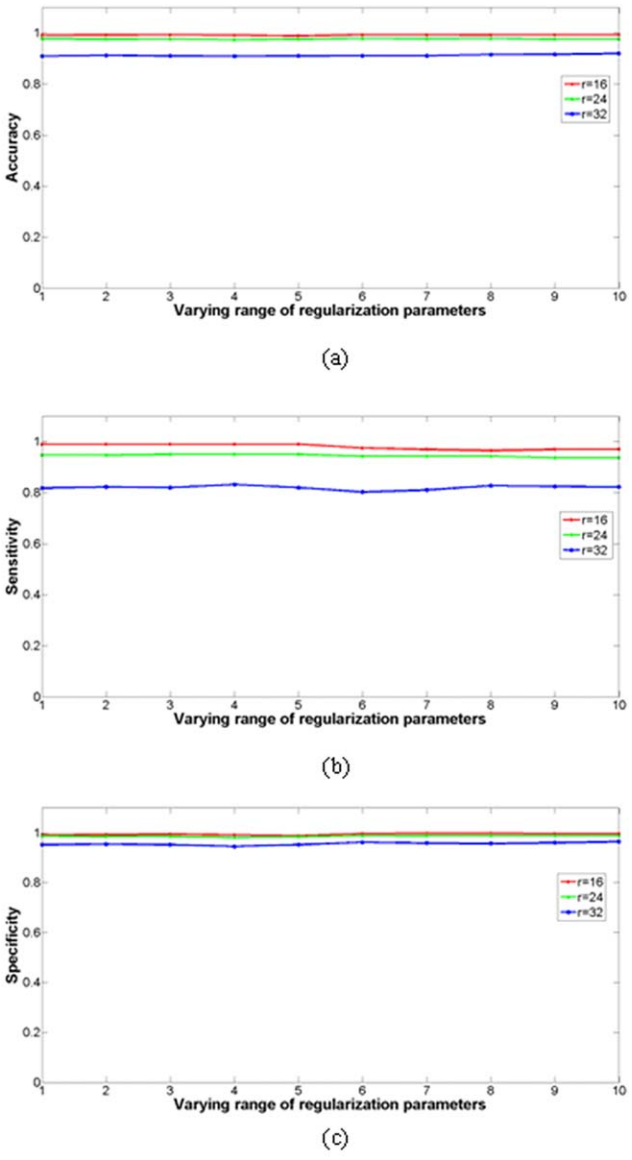

Figure 3.

Dependence of the JGMSS in terms of: (**a**) accuracy, (**b**) sensitivity, and (**c**) specificity on varying ranges (i.e., the first 10 out of 50 combinations of λ_1 and λ_2 are removed sequentially) of regularization parameters. The independence of the JGMSS to the choice of initial set of regularization parameters can be easily identified by the stability of accuracy and sensitivity calculated from the three estimated networks (r = 16, 24, 32), corresponding to red, green, blue lines, respectively. [Color figure can be viewed in the online issue, which is available at wileyonlinelibrary.com.]

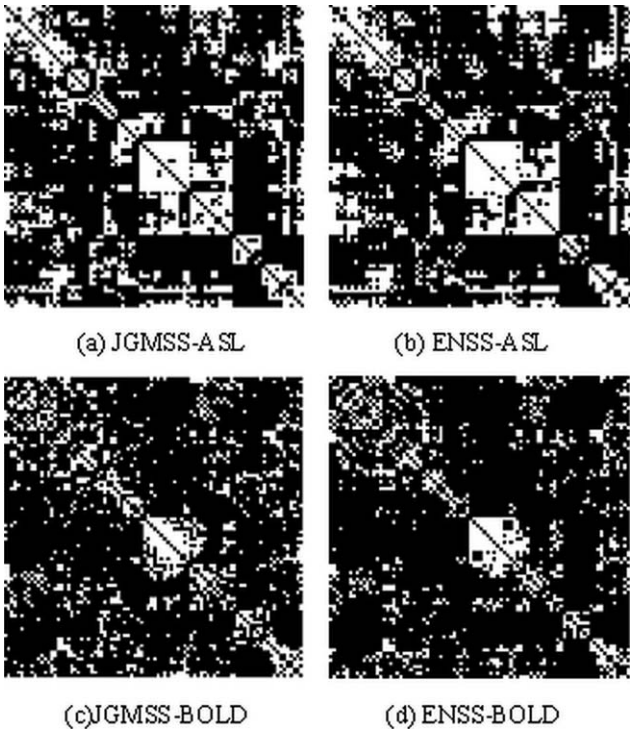

Figure 4.

Estimation of group functional networks from in vivo ASL data using (**a**) JGMSS and (**b**) ENSS (top row), as well as from BOLD data using (**c**) JGMSS and (**d**) ENSS (bottom row). Networks estimated from ASL and BOLD data using JGMSS and ENSS have equivalent network density (black = 0, white = 1).

controlling confounding variations while minimally compromising biological variation; this is achieved by imposing the biologically-plausible joint sparse constraint. Importantly, a stability selection method is then introduced to circumvent the issue of choosing optimal regularization parameters [Meinshausen and Buhlmann, 2010]. The proposed method, therefore, can robustly estimate functional networks from a group of subjects by seeking sparse constrained solutions.

While a recent study proposed to estimate group functional networks using a mixed norm L_{21} [Varoquaux et al., 2010b], we applied two separate penalties, L_1 and L_{21}, to all precision matrices of the group in the current study; the two regularization parameters can then be flexibly tuned to achieve more robust estimation of networks. Specifically, in contrast to the two-fold cross-validation procedure used in that study, our proposed method employs a more straightforward stability selection method to directly estimate the group functional networks by avoiding the dilemma of explicit model selection [Meinshausen and Buhlmann, 2010].

In addition, Varoquaux et al. have also proposed a novel method that is conducted at group-level but is suitable for intersubject comparison of functional networks [Varoquaux et al., 2010a]. In that study, they employ Ledoit-Wolf shrinkage, i.e. L_2 regularization, to estimate the residuals of individual correlation matrices in the space tangent to the mean covariance matrix of the control group. Nonparametric sampling can then be used to define a null distribution for the residuals of individual connectivity matrices, thereby accounting for projection error. For each patient, univariate analyses on such parameters are then conducted to test if the network is significantly different from the control group, and it has been demonstrated that patients can be better separated from controls by using this approach. Given that L_2 regularization is employed in that method, non-sparse networks can be achieved; in contrast, we aim to estimate sparse functional networks.

Estimated group functional networks from all of the simulated datasets have shown that the JGMSS can achieve consistently higher accuracy and sensitivity than ENSS across the range of r values used, despite relatively fewer time points than typical fMRI data (56 vs. 100 or more) [De Luca et al., 2006].

JGMSS and ENSS estimated similar functional networks, and with similar network densities, for the in vivo data. A previous study of functional networks using ENSS [Ryali et al., 2012] had demonstrated this method's capability in reliably detecting brain networks; our results confirm these findings, as well as provide evidence that JGMSS can also be used for reliably detecting brain networks. Despite the similarity between the network densities from JGMSS and ENSS in our in vivo data, more detailed analysis revealed node-degree disparities between the results from the two methods (see Fig. 7 and Table I). While there is no ground-truth for assessing the results from in vivo data, the fact that JGMSS is more capable than ENSS of detecting well-accepted hub regions (for both ASL and BOLD data) corroborates the simulation findings that JGMSS estimates group functional networks more reliably than ENSS.

It should be noted that number of hub regions detected using JGMSS is different between our ASL and BOLD data, i.e. more hub regions are detected from BOLD than from ASL data. A few reasons might account for this difference. Firstly, while all 90 brain regions were considered for the BOLD data, only 84 regions were included in ASL data [Liang et al., 2014]. Such difference is likely to result in a difference in the final hub regions detected. In addition, ASL and BOLD fMRI are based on different (although related) underlying sources of signal change; ASL data provide direct physiological measurement of cerebral blood flow based on a non-BOLD contrast, while BOLD signal is measured in arbitrary units that are a complex interaction of CBV, CBF and CMRO2 [Boxerman et al., 1995]. Finally, different acquisition parameters (such as TR, number of time points, voxel size, etc.) employed for ASL and BOLD fMRI might also contribute to the difference in detecting hub regions.

The superiority of JGMSS over ENSS is also evidenced by the consistently higher R^2 values for the fitted degree distributions from ASL and BOLD networks Note that the

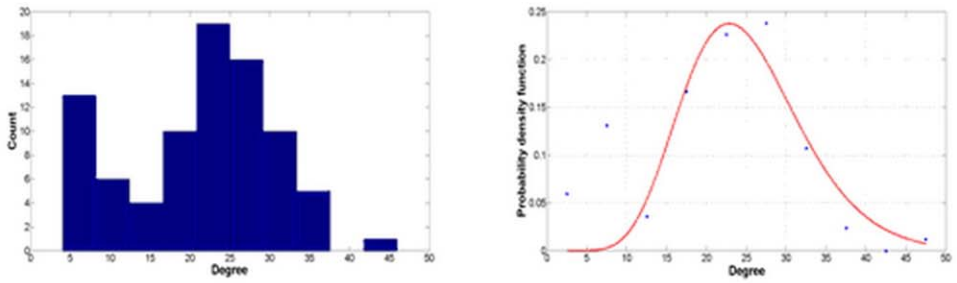

(a) ASL JGMSS, $R^2 = 0.66$

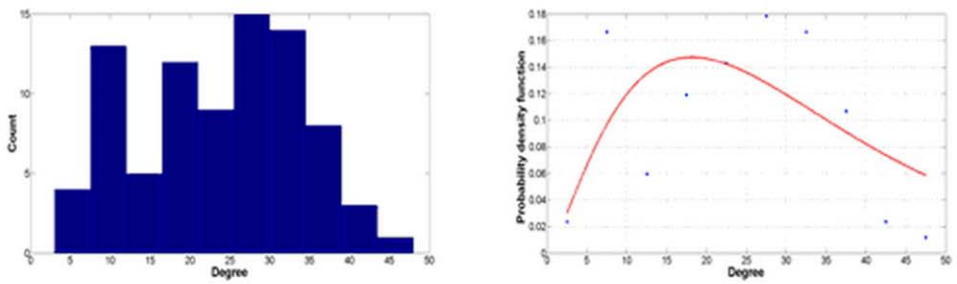

(b) ASL ENSS, $R^2 = 0.42$

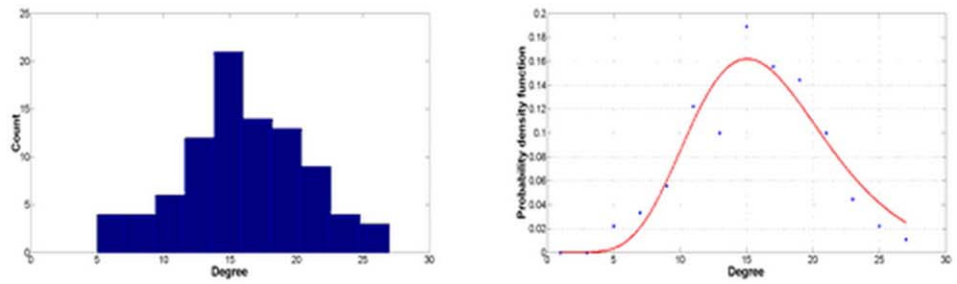

(c) BOLD JGMSS, $R^2 = 0.9$

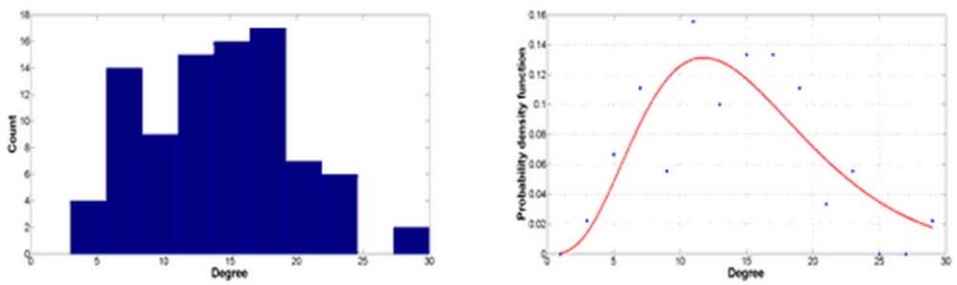

(d) BOLD ENSS, $R^2 = 0.72$

Figure 5.

Degree distributions (left column) and their fitting outcomes (right column) of functional networks extracted from: (**a**) ASL data using JGMSS; (**b**) ASL data using ENSS; (**c**) BOLD data using JGMSS; (**d**) BOLD data using ENSS. Extracted functional networks using JGMSS were better characterized by exponentially truncated power-law degree distribution (solid lines) than ENSS, evidenced by consistently higher R^2 values. [Color figure can be viewed in the online issue, which is available at wileyonlinelibrary.com.]

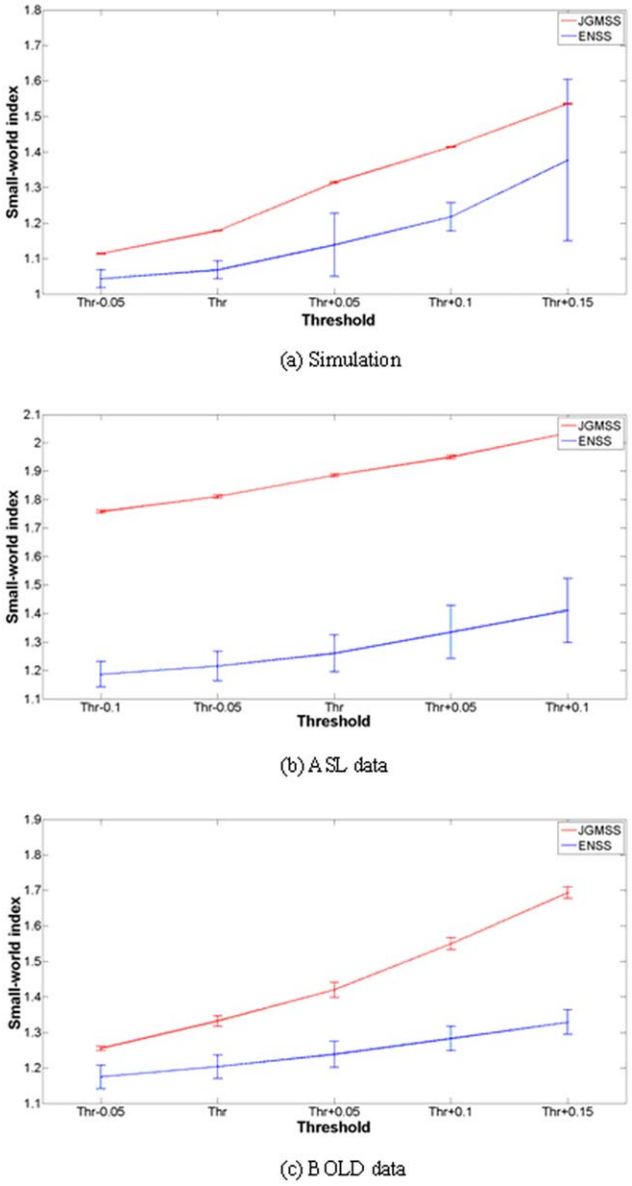

Figure 6.

Means and standard deviations of small-world indices calculated from groups, with each small-world index derived from an individual network. (**a**) Simulation, (**b**) ASL and (**c**) BOLD data across ranges of P_{thr}. Reduced intersubject variability is achieved by using JGMSS (red line) than by using ENSS (blue line) for all cases. [Color figure can be viewed in the online issue, which is available at wileyonlinelibrary.com.]

lower R^2 values obtained from ASL data than from BOLD data (for both JGMSS and ENSS methods) are mainly due to the associated fewer time points and lower SNR for ASL data.

As with previous studies, our results show that all networks estimated from simulated, ASL and BOLD fMRI data possess small-world properties, i.e.$\sigma > 1$, regardless of the methods employed [Achard et al., 2006; Liang et al., 2012b, 2014]. Importantly, JGMSS achieves much less intersubject variability regardless of data origin than does ENSS. While the intersubject variability of simulated and ASL data is very low when JGMSS is applied, the variability of BOLD data is relatively larger, which is consistent with previous findings that ASL tends to produce less intersubject variability compared to BOLD [Aguirre et al., 2002; Wang et al., 2003]. Importantly, the capability of JGMSS in controlling for confounding variations is of significance for studies involving group comparisons. Specifically, the reduction of confounding variations for individual networks that are simultaneously estimated by employing the joint sparse constraint can achieve either higher statistical power or a lower required minimum sample size. It should be emphasized in this context that the biologically-plausible sparse constraint used by JGMSS aims to control for intersubject variability caused by confounding variations, mainly characterized by non-sparsity, while minimally compromising true biological variations (which are unlikely to be removed by a sparse constraint). Such biological intersubject variations are important for interpretation of findings in inter-group comparisons, given that differences in connections with higher variability will have lower detection sensitivity.

Note that while the results from JGMSS have much lower variability, there were still a small number of connections with relatively high variability (see Supporting Information Fig. S1). This might be related to higher intersubject biological variability for those connections. However, future studies are required to determine the source(s) of this residual variability.

Given that choosing appropriate thresholds remains an open question, PCER was employed in the current study to determine the threshold for stability selection by controlling the total number of falsely selected connections, i.e., by setting the false positive rates below a certain level. Simulated results have shown that JGMSS tends to estimate more true connections, but comparable false connections, compared to ENSS; thus, it achieves higher accuracy and sensitivity. Furthermore, our simulations demonstrated that estimated networks had stable accuracy and sensitivity rates across a varying range of regularization parameters, thus indicating the robustness of JGMSS, with very low sensitivity to the choice of initial set of regularization parameters.

Methodological Issues

In this study, all networks investigated contain only binary edges, indicating whether a pair of nodes are connected (edge = 1) or not (edge = 0). This is a consequence of the method's sparse constraint approach. There has been, however, increasing interest in investigating weighted-networks, which can provide a more comprehensive description. Although this represents a limitation for the

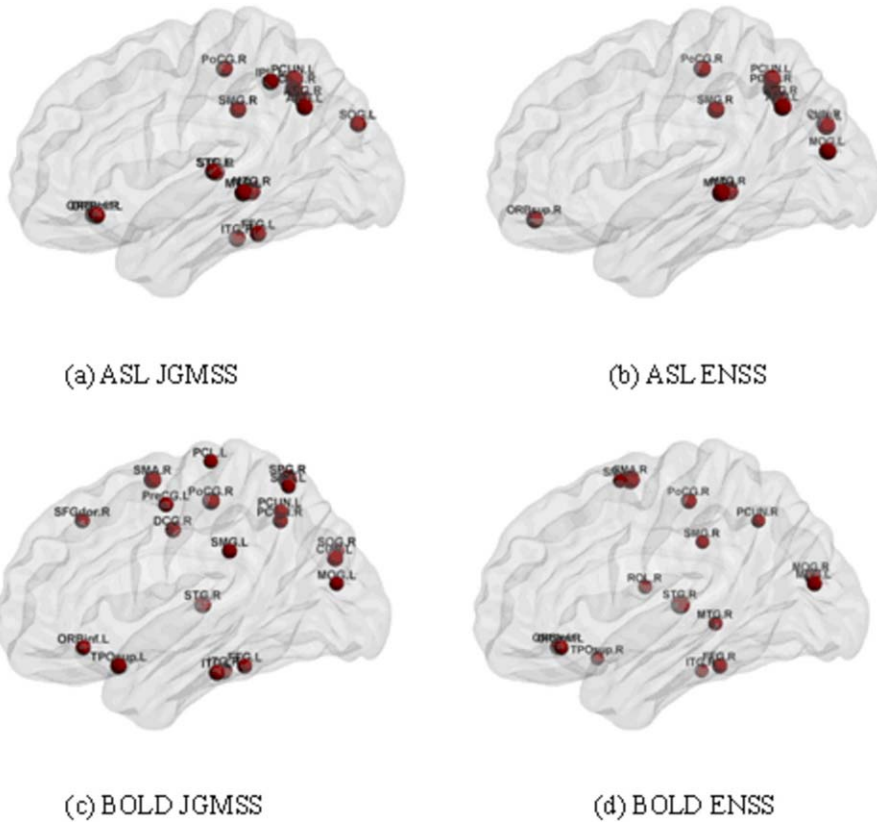

Figure 7.

Sagittal view of detected brain hub regions from in vivo data. (top) ASL data using (**a**) JGMSS and (**b**) ENSS; (bottom) BOLD data using (**c**) JGMSS and (**d**) ENSS. Hub regions are mapped onto the standard MNI template by using the BrainNet Viewer software. JGMSS detected more brain hub regions than ENSS for both ASL and BOLD data (see Table I for details). ANG: angular gyrus, CUN: cuneus, DCG: dorsal cingulated gyrus, FG: fusiform gyrus, IPL: inferior parietal lobule, ITG: inferior temporal gyrus, MOG: middle occipital gyrus, MTG: middle temporal gyrus, ORBinf: inferior frontal gyrus-orbital, ORBsup: orbitofrontal cortex-superior, PCL: paracentral lobule, PreCG: precentral gyrus, PoCG: postcentral gyrus, ROL: rolandic operculum, SFG: superior frontal gyrus, SOG: superior occipital gyrus, STG: superior temporal gyrus, SPG: superior parietal gyrus, SMA: supplementary motor area, SMG: supramarginal gyrus. [Color figure can be viewed in the online issue, which is available at wileyonlinelibrary.com.]

JGMSS method, it should be noted that binary networks have constituted by far the main focus to date of network analyses using graph theoretical approaches.

The proposed JGMSS method reduces intersubject variability. While JGMSS exclusively aims to control confounding variation, it is not clear whether biological variation is also unfavorably affected. However, given that brain networks are sparse [Achard and Bullmore, 2007; Bullmore and Sporns, 2012; Liang et al., 2015], the biological constraint of sparsity employed by JGMSS is likely to favorably push the estimated network towards the correct estimate, i.e. it achieves robust estimation of networks by favorably controlling for confounding variation, mainly characterized by non-sparsity, while minimally affecting biological variation. Further investigation is however warranted to characterize this effect. It is also worth noting that while our proposed method can largely control confounding variations mainly characterized by non-sparsity (such as random noise and motion artifacts), through sparse regularization, it might not be feasible to effectively remove those confounding variations caused by sources of physiological noise given their sparsity properties [Churchill et al., 2012]. Nevertheless, this by no means indicates that the proposed method is incapable of estimating brain networks, but rather suggests that further steps to remove physiological noise, such as RETROICOR [Glover et al., 2000] or PHYCAA [Churchill et al., 2012] should be employed to achieve more reliable results by ensuring that "sparse-like" confounding variations are also controlled during the preprocessing step.

A limitation of the current study therefore is that we did not apply specific preprocessing steps to remove

TABLE I. Differences in detected hub brain regions from in vivo ASL and BOLD data using JGMSS and ENSS

	ASL		BOLD	
ROI name	JGMSS	ENSS	JGMSS	ENSS
Precuneus (L)	Hub	Hub	Hub	No
Precuneus (R)	Hob	Hub	Hub	Hub
Middle temporal gyrus (L)	Hub	Hub	No	No
Middle temporal gyrus (R)	Hub	Hub	No	Hub
Superior temporal gyrus (L)	Hub	No	No	No
Superior temporal gyrus (R)	Hub	No	Hub	Hub
Inferior temporal gyrus (L)	No	No	Hub	No
inferior temporal gyrus (R)	Hub	No	Hub	Hub
Inferior parietal lobule (L)	Hub	No	No	No
Superior parietal gyrus (L)	No	No	Hub	No
Superior parietal gyrus (R)	No	No	Hub	No
Precentral gyrus (L)	No	No	Hub	No
Postcentral gyrus (R)	Hub	Hub	Hub	Hub
Inferior frontal gyrus-orbital(L)	Hub	No	Hub	Hub
Inferior frontal gyrus-orbital(R)	Hub	No	No	Hub
Superior frontal gyrus-dorsal (R)	No	No	Hub	No
Dorsal cingulated gyrus (R)	No	No	Hub	No
Supramarginal gyrus (L)	No	No	Hub	No
Supramarginal gyrus (R)	Hub	Hub	No	Hub
Supplementary motor area (L)	N/A	N/A	No	Hub
Supplementary motor area (R)	N/A	N/A	Hub	Hub
Paracentral lobule (L)	N/A	N/A	Hub	No
Middle occipital gyrus (L)	No	Hub	Hub	Hub
Middle occipital gyrus (R)	No	No	No	Hub
Superior occipital gyrus (L)	Hub	No	No	No
Superior occipital gyrus (R)	No	No	Hub	No
Fusiform gyrus (L)	Hub	No	Hub	No
Fusiform gyrus (R)	No	No	No	Hub
Rolandic operculum (R)	No	No	No	Hub
Temporal pole-superior (L)	No	No	Hub	No
Temporal pole-superior (R)	No	No	No	Hub
Angular gyrus (L)	Hub	Hub	No	No
Angular gyrus (R)	Hub	Hub	No	No
Cuneus (L)	No	Hub	Hub	No
Cuneus (R)	No	Hub	No	No
Orbitofrontal cortex-superior (R)	No	Hub	No	No

The brain region marked with red color was erroneously detected as a hub region by using ENSS, but it does not correspond to a known hub region. N/A indicates brain regions that were not included in the parcellation of ASL data.

physiological noise, and this might have compromised our estimations of brain networks. Importantly, it is worth noting that since the same preprocessing steps were applied to both methods compared here, i.e. JGMSS and ENSS, the absence of physiological noise removal should not alter our conclusions.

We have focused here on group-level analysis. While group comparisons of brain networks reveal common mechanisms underlying disease conditions, comparisons at individual-level can explicitly take account of intersubject variability as related to biological variations. As a result, the development of robust methods to model disease at individual level attracted increasing interest. However, it should be noted that intersubject variability as related to confounding variations can largely compromise such individual studies unless such variability can be appropriately accounted for; this confounding effect can be particularly important with noisy fMRI data.

CONCLUSION

A novel sparse partial correlation method for robust estimation of group functional networks has been described. The proposed method (JGMSS) simultaneously estimates individual networks from a homogeneous group by using a joint sparse constraint method; a stability selection method was further employed to circumvent the issue of choosing the optimal model, i.e., the optimal regularization parameters. By applying JGMSS and ENSS to simulated data, it has been demonstrated that the JGMSS achieves consistently higher accuracy and sensitivity across connections. The better performance of JGMSS compared to ENSS has been further corroborated by the in vivo fMRI data (ASL and BOLD), through extracting networks that are better characterized by the exponentially truncated power law model and identifying a greater number of known hub regions. More importantly, JGMSS yields much less intersubject variability than ENSS, which is beneficial for studies involving group comparisons. Note that the performance of JGMSS on both simulations and ASL data indicates that JGMSS is especially robust for low SNR data and a relative small number of time points. The reported findings suggest that the proposed method provides a robust tool for characterizing brain networks at group-level.

REFERENCES

Achard S, Bullmore E (2007): Efficiency and cost of economical brain functional networks. PLoS Comput Biol 3:e17.

Achard S, Salvador R, Whitcher B, Suckling J, Bullmore E (2006): A resilient, low-frequency, small-world human brain functional network with highly connected association cortical hubs. J Neurosci 26:63–72.

Aguirre GK, Detre JA, Zarahn E, Alsop D (2002): Experimental design and the relative sensitivity of BOLD and perfusion fMRI. Neuroimage 15:488–500.

Akaike H (1974): A new look at the statistical model identification. IEEE Trans Automat Control 19:716–723.

Aslan S, Xu F, Wang PL, Uh J, Yezhuvath US, Van Osch M, Lu H (2010): Estimation of labeling efficiency in pseudocontinuous arterial spin labeling. Magn Reson Med 63:765–771.

Boxerman JL, Bandettini PA, Kwong KK, Baker JR, Davis TL, Rosen BR, Weisskoff RM (1995): The intravascular contribution to fMRI signal change: Monte Carlo modeling and diffusion-weighted studies in vivo. Magn Reson Med 34:4–10.

Boyd S, Parikh N, Peleato B, Eckstein J (2010): Distributed optimization and statistical learning via the alterating direction method of multipliers. Found Trends Mach Learn 3:1–122.

Buckner RL, Krienen FM, Castellanos A, Diaz JC, Yeo BT (2011): The organization of the human cerebellum estimated by intrinsic functional connectivity. J Neurophysiol 106:2322–2345.

Bullmore E, Sporns O (2012): The economy of brain network organization. Nat Rev Neurosci 13:336–349.

Calamante F, Thomas DL, Pell GS, Wiersma J, Turner R (1999): Measuring cerebral blood flow using magnetic resonance imaging techniques. J Cereb Blood Flow Metab 19:701–735.

Chiquet J, Grandvalet Y, Ambroise C (2011): Inferring multiple graphical structures. Statistics and Computing 21:537–553.

Chuang KH, Van Gelderen P, Merkle H, Bodurka J, Ikonomidou VN, Koretsky AP, Duyn JH, Talagala SL (2008): Mapping resting-state functional connectivity using perfusion MRI. Neuroimage 40:1595–1605.

Churchill NW, Yourganov G, Spring R, Rasmussen PM, Lee W, Ween JE, Strother SC (2012): PHYCAA: Data-driven measurement and removal of physiological noise in BOLD fMRI. Neuroimage 59:1299–1314.

Danaher P, Wang P, Witten DM (2014): The joint graphical lasso for inverse covariance estimation across multiple classes. J R Stat Soc Ser B 76:373–397.

DE Luca M, Beckmann CF, De Stefano N, Matthews PM, Smith SM (2006): fMRI resting state networks define distinct modes of long-distance interactions in the human brain. Neuroimage 29:1359–1367.

Dempster AP (1972): Covariance selection. Biometrics 28:157–175.

Eichler M, Dahlhaus R, Sandkuhler J (2003): Partial correlation analysis for the identification of synaptic connections. Biol Cybernet 89:289–302.

Garcia DM, Duhamel G, Alsop DC (2005): Efficiency of inversion pulses for background suppressed arterial spin labeling. Magn Reson Med 54:366–372.

Glover GH, Li TQ, Ress D (2000): Image-based method for retrospective correction of physiological motion effects in fMRI: RETROICOR. Magn Reson Med 44:162–167.

Gonzalez-At JB, Alsop DC, Detre JA (2000): Cerebral perfusion and arterial transit time changes during task activation determined with continuous arterial spin labeling. Magn Reson Med 43:739–746.

Guo J, Levina E, Michailidis G, Zhu J (2011): Joint estimation of multiple graphical models. Biometrika 98:1–15.

Hampson M, Peterson BS, Skudlarski P, Gatenby JC, Gore JC (2002): Detection of functional connectivity using temporal correlations in MR images. Hum Brain Mapp 15:247–262.

Hansen LK, Larsen J, Nielsen FA, Strother SC, Rostrup E, Savoy R, Lange N, Sidtis J, Svarer C, Paulson OB (1999): Generalizable patterns in neuroimaging: how many principal components? Neuroimage 9:534–544.

Hayasaka S, Laurienti PJ (2010): Comparison of characteristics between region-and voxel-based network analyses in resting-state fMRI data. Neuroimage 50:499–508.

Latora V, Marchiori M (2001): Efficient behavior of small-world networks. Phys Rev Lett 87:198701.

Liang X, Tournier JD, Masterton R, Connelly A, Calamante F (2012a): A k-space sharing 3D GRASE pseudocontinuous ASL method for whole-brain resting-state functional connectivity. Int J Imaging Syst Technol 22:37–43.

Liang X, Wang J, Yan C, Shu N, Xu K, Gong G, He Y (2012b): Effects of different correlation metrics and preprocessing factors on small-world brain functional networks: A resting-state functional MRI study. PLoS One 7:e32766.

Liang X, Connelly A, Calamante F (2013). A novel efficient denoising method for ASL data: Assessment using voxel-wise network analysis. In: Proceedings of the ISMRM 21th Annual Meeting. Salt Lake City, UT, USA, pp 1772.

Liang X, Connelly A, Calamante F (2014): Graph analysis of resting-state ASL perfusion MRI data: Nonlinear correlations among CBF and network metrics. Neuroimage 87:265–275.

Liang X, Connelly A, Calamante F (2015): Voxel-Wise Functional Connectomics Using Arterial Spin Labeling Functional Magnetic Resonance Imaging: The Role of Denoising. Brain Connect 5:543–553.

Liao XH, Xia MR, Xu T, Dai ZJ, Cao XY, Niu HJ, Zuo XN, Zang YFHEY (2013): Functional brain hubs and their test-retest reliability: a multiband resting-state functional MRI study. Neuroimage 83:969–982.

Maslov S, Sneppen K (2002): Specificity and stability in topology of protein networks. Science 296:910–913.

Meinshausen N, Buhlmann P (2010): Stability selection. J R Stat Soc Ser B 72:417–473.

Ng B, Varoquaux G, Poline JB, Thirion B (2013): A novel sparse group Gaussian graphical model for functional connectivity estimation. Inf Process Med Imaging 23:256–267.

Peng J, Wang P, Zhou NF, Zhu J (2009): Partial correlation estimation by joint sparse regression models. J Am Stat Assoc 104:735–746.

Rasmussen PM, Hansen LK, Madsen KH, Churchill NW, Strother SC (2012): Model sparsity and brain pattern interpretation of classification models in neuroimaging. Pattern Recognit 45:2085–2100.

Ryali S, Chen T, Supekar K, Menon V (2012): Estimation of functional connectivity in fMRI data using stability selection-based sparse partial correlation with elastic net penalty. Neuroimage 59:3852–3861.

Salvador R, Suckling J, Coleman MR, Pickard JD, Menon D, Bullmore E (2005): Neurophysiological architecture of functional magnetic resonance images of human brain. Cereb Cortex 15:1332–1342.

Schwartz G (1978): Estimating the dimension of a model. Ann Stat 19:461–464.

Simpson SL, Moussa MN, Laurienti PJ (2012): An exponential random graph modeling approach to creating group-based representative whole-brain connectivity networks. Neuroimage 60: 1117–1126.

Sporns O, Kotter R (2004): Motifs in brain networks. PLoS Biol 2:e369.

Sporns O, Zwi JD (2004): The small world of the cerebral cortex. Neuroinformatics 2:145–162.

Stam CJ (2014): Modern network science of neurological disorders. Nat Rev Neurosci 15:683–695.

Stam CJ, Reijneveld JC (2007): Graph theoretical analysis of complex networks in the brain. Nonlinear Biomed Phys, 1:3

Tibshirani R (1996): Regression shrinkage and selection via the lasso. J R Stat Soc Ser B 58:267–278.

Tzourio-Mazoyer N, Landeau B, Papathanassiou D, Crivello F, Etard O, Delcroix N, Mazoyer B, Joliot M (2002): Automated anatomical labeling of activations in SPM using a macroscopic anatomical parcellation of the MNI MRI single-subject brain. Neuroimage 15:273–289.

Varoquaux G, Baronnet F, Kleinschmidt A, Fillard P, Thirion B (2010a): Detection of brain functional-connectivity difference in

post-stroke patients using group-level covariance modeling. Med Image Comput Comput Assist Interv 13:200–208.

Varoquaux G, Gramfort A, Poline JB, Thirion B. (2010b): Brain covariance selection: Better individual functional models using population prior. Advances in Neural Information Processing Systems, Vancouver, Canada.

Wang J, Aguirre GK, Kimberg DY, Roc A, Detre JA (2003): Arterial spin labeling perfusion fMRI with very low task frequency. Magn Reson Med 49:796–802.

Watts Dj, Strogatz SH (1998): Collective dynamics of 'small-world' networks. Nature 393:440–442.

Witten Dm, Tibshirani R (2009): Covariance-regularized regression and classification for high dimensional problems. J R Stat Soc Ser B 71:615–636.

Zhang Y, Shen X (2010): Model selection procedure for high-dimensional data. Stat Anal Data Min 3:350–358.

Zou H, Hastie T (2005): Regularization and variable selection via the elastic net. J R Stat Soc Ser B 67:301–320.